Beam-Ion Instability in the Fermilab Linac

K.Y. Ng and M. Popovic

Fermi National Accelerator Laboratory, P.O. Box 500, Batavia, IL 60510

Abstract

Beam-ion instabilities were observed in the 750 keV transfer line of the Fermilab linac when various gases were injected and the pressure was raised to between 1×10^{-5} and 1×10^{-4} Torr. The collective resonant frequencies recorded, of the order of 1 MHz, are in qualitative agreement with the linear theory of fast beam-ion instability proposed by Raubenheimer and Zimmermann [1], but fail to follow the $A^{-1/2}$ dependency, where A is the ion mass number, and have the tendency to increase with pressure. The observed growth times along the beam are in rough agreement with those provided by the theory, although the latter tend to be somewhat larger.

1 INTRODUCTION

Fast transverse oscillations with large amplitudes were observed [2] in the H^- beam in the 750 keV transfer line of the Fermilab linac in 1988 when the vacuum pressure was raised to 7×10^{-6} Torr to reduce the effect of space charge on the beam [3, 4] and thereby reduce the effective emittance entering the linac. In order not to degrade the performance of the 8 GeV booster, into which the linac injects, this transverse instability has been avoided by choosing the operating vacuum pressure to be 2.65×10^{-6} Torr. The instability observed resembles the fast beam-ion instability proposed by Raubenheimer and Zimmermann [1], where individual ions last only for a single passage of the particle beam and need not be trapped. The ions generated by the beam accumulate as the beam passes by and oscillate in the transverse direction causing a growth of the initial perturbation of the beam. The result is a coherent oscillation with growing amplitudes for the coupled beam-ion system.

An experiment was performed at the 750 keV transfer line in 2000 in order to further understand the instability previously observed [5]. Many different residual gases were used and the vacuum pressure was varied. In this paper, we are going to analyze the experimental data and see whether the resonant frequencies of the coupled beam-ion transverse oscillation and growth times along the beam conform with the predictions of the linear theory of the fast beam-ion instability.

2 THE EXPERIMENT

Figure 1 shows the 750 keV transfer line into the main linac. Different gases like hydrogen, helium, nitrogen, argon, and krypton, were injected through the bleeding valve. The gas pressure was controlled by adjusting the rate of

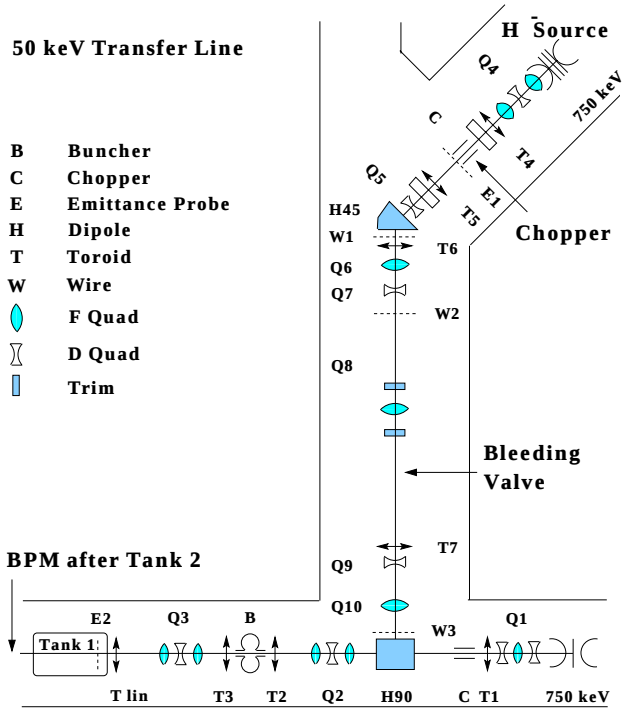

Figure 1: The 750 keV transfer line of the Fermilab linac. The length is ~ 10 m from the chopper C to the entry into the linac. Beam current measurements are made by a toroid monitor between Tank 1 and Tank 2, and again further downstream.

flow of gas at the bleeding valve while vigorously pumping at the large ion pumps near the chopper C and the entrance into Tank 1 as well as a small ion pump near the bleeding valve. The pressure monitored near the three ion pumps showed steady readings. In this way the vacuum pressure could be varied between 1×10^{-5} and 1×10^{-4} Torr, while the normal operating vacuum pressure has been 2.65×10^{-6} Torr. A toroidal monitor near the exit of Tank 1 and entrance of Tank 2 measured the beam current. We see in Fig. 2 that the beam current in the transfer line (top) decreases with pressure. This is mostly due to the stripping of the electron on H^- by collision with the gas particles so that the resulting neutral H particles could not follow the dipole bend H90 into the current monitor. Another current monitor downstream measured the beam current in the linac downstream (bottom). The smaller values observed represent beam loss.

A 750 keV H^- beam chopped to the length of $\tau_b = 35\ \mu$s entered the transfer line. Its center position was picked up by the beam-position monitor (BPM) after Tank 2. The signals were recorded using a LeCroy scope and the spec-

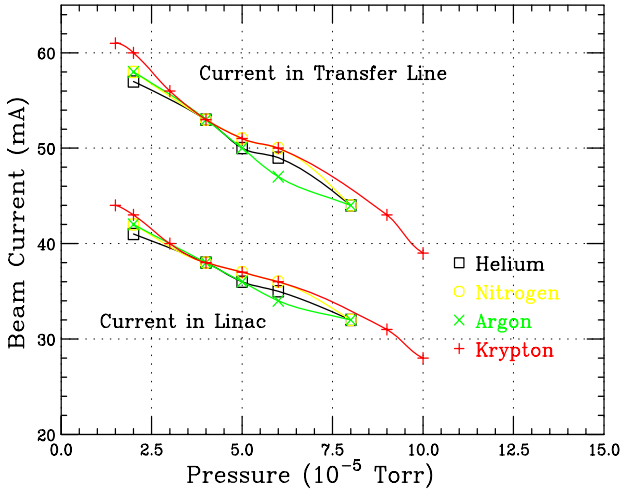

Figure 2: (color) Beam current in the transfer line (top) measured by toroids between Tank 1 and Tank 2, and further downstream in the linac (bottom). The drop in beam current at higher vacuum pressure is probably due to the stripping of the electron on the H^- by the gases injected.

tral content was obtained numerically using FFT. To lower the noise level, measurements were averaged over approximately 20 beam pulses. To avoid any signal not related with the beam oscillation, only the last 20 μs of the beam pulse were Fourier analyzed. There was no noticeable difference between displacement signals in the horizontal and vertical planes, so all data were taken in the horizontal plane only.

A typical set of results for nitrogen at 3×10^{-5} Torr is shown in the top plot of Fig. 3, where the first two traces correspond to the beam intensity and the horizontal beam position, respectively. The 4th trace is the FFT of the beam position for the last 20 μs of the beam, while the 3rd trace depicts the average of 23 FFT beam pulses. We can clearly see a resonant frequency of ~ 0.5 MHz. As the gas pressure was increased to 8×10^{-5} Torr in the lower plot of Fig. 3, the resonant signal is broadened and spreads out to higher frequencies.

Figure 4 shows the BPM signals for the horizontal oscillations of the H^- beam when argon is introduced. We see rapid growth in oscillation amplitude along the beam. The growth becomes much faster as the gas pressure is increased from 3×10^{-5} to 1×10^{-4} Torr. We also notice that saturation is reached very soon and the growth stops.

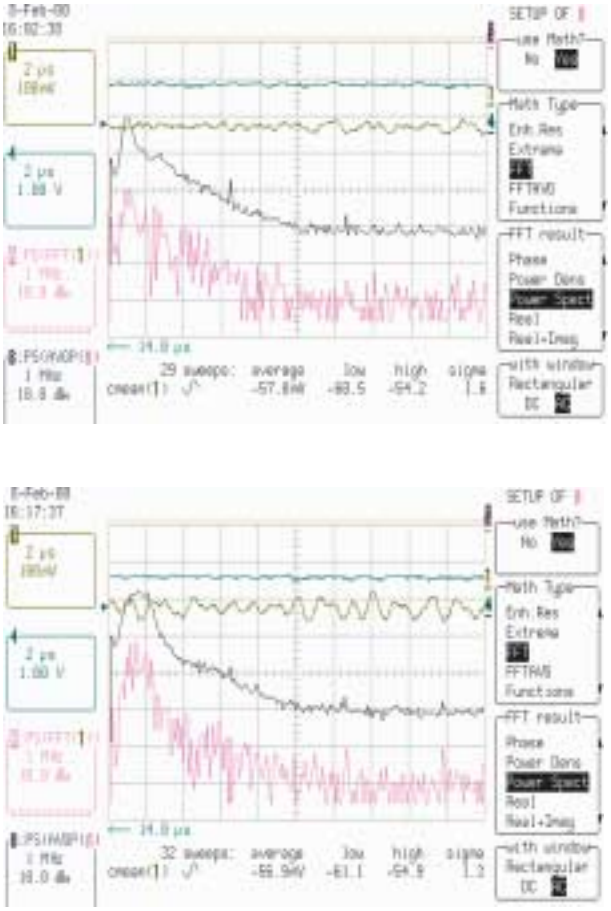

Figure 3: (color) Beam intensity (1st trace) and beam horizontal displacement (2nd trace) from the 14th μs at 2 μs per division, when the injected gas is nitrogen at 3×10^{-5} Torr (top) and 8×10^{-5} Torr (bottom). The 4th trace is the FFT at 1 MHz per division of the last 20 μs of the beam horizontal displacement. The third trace is the FFT averaged over 20 beam pulses. As pressure increases, the resonant peak becomes broadened and moves towards higher frequencies.

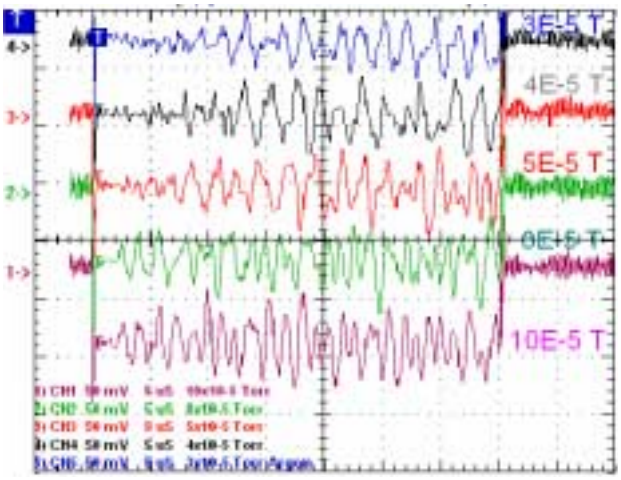

Figure 4: (color) Horizontal displacements of the 35 μs H^- beam in an argon gas environment at various pressures. An instability is observed and the beam displacements become saturated. The growth rate increases with gas pressure.

3 ANALYSIS

3.1 Ionization Cross Section

When the velocity of the incident particle is much larger than the velocity of the electron inside the target atom about to be ionized, the impulse approximation can be used. Our experiment condition satisfies this criterion. The ionization energy of the electron in the outermost shell is given by

$$U = U_0 \left(\frac{Z}{n}\right)^2_{\text{eff}} \tag{3.1}$$

Table 1: Ionization cross sections of various gases by 750 keV H^-. Velocities of electrons in the outermost shells of the gas atoms are estimated by an effective value of Z/n due to screening, where Z is the atomic number of the gas element and n the principal quantum number of the electron. Values of M^2 and C are from experiments [8].

	H	He	N	Ar	Kr
Atomic number Z	1	2	7	18	36
Atomic mass number A	1	4	14	40	84
Ionization energy U (eV)	13.6	24.6	14.5	15.6	14.0
Effective ratio $(Z/n)^2_{\rm eff}$	1.00	1.8088	1.0662	1.1618	1.029
Electron velocity in outermost shell v_e/c	0.0073	0.0098	0.0075	0.0079	0.0074
Target variable in Eq. (3.3) M^2	0.695	0.738	3.73	4.22	6.09
Target variable in Eq. (3.3) C	8.115	7.056	34.84	37.93	52.38
Ionization cross section Σ (Mb)	42.71	27.03	126.2	126.2	154.5

where Z is the atomic number of the gas element and n is the principal quantum number of the outermost shell of the gas atom. Here, $U_0 = hcR_\infty = 13.605$ eV is Rydberg energy or the ionization energy of hydrogen, $h = 6.582 \times 10^{-22}$ MeV-s is the Planck constant, and c is the velocity of light. Since the electrons in the inner shells shield the electric charges of the nucleus, the effective ratio $(Z/n)^2_{\rm eff}$ is less than the actual $(Z/n)^2$. The effective ratios for the various gases estimated from Eq. (3.1) are listed in Table 1. The velocity v_e of the electron in the outermost shell is

$$v_e = v_0 \left(\frac{Z}{n}\right)_{\rm eff} \tag{3.2}$$

where $v_0 = r_e c/\lambda\!\!\!^{-}_e = 0.0073$ is the velocity of the electron in the hydrogen atom, $r_e = 2.818 \times 10^{-18}$ m is the electron classical radius, and $\lambda\!\!\!^{-}_e = \hbar/(m_e c) = 3.86159323 \times 10^{-13}$ m is the reduced electron Compton wavelength. We see that the velocities of the electron in the outermost cells of the gas atoms in this experiment are roughly $0.0073c$ to $0.0098c$, which are indeed much less than the velocity $\beta c = 0.040c$ of the 750 keV H^-.

In the impulse approximation, the bound electrons are knocked out by a sudden transfer of energy from the incident particle. Therefore, the ionization cross section does not depend very much on the ionization energy of the target atom. From the work of Bethe [6, 7], the ionization cross section in the first Born approximation can be written as

$$\Sigma = 4\pi\lambda\!\!\!^{-2}_e \left[M^2\left(\frac{\ln\beta^2\gamma^2}{\beta^2} - 1\right) + \frac{C}{\beta^2}\right], \tag{3.3}$$

where β and γ are the Lorentz factors of the incident particle with the target at rest. The two variables M^2 and C depend on the generalized oscillator strength inside the target atom for all the transitions involved. Notice that this expression depends on the incident particle only through its *velocity*, which is an important consequence of the Born approximation and has been verified by many experiments [8]. The experimental values of M^2 and C as well as the cross sections of the gases involved are listed in Table 1.

3.2 Resonant Frequencies

The ionized gases are trapped by the H^- beam and oscillate about the H^- beam. The resonant angular frequency is given by

$$\omega_i = \sqrt{\frac{4\lambda_b r_p c^2}{a_h(a_v + a_h)A}}\,, \tag{3.4}$$

where λ_b is the linear beam density, $r_p = 1.53470 \times 10^{-18}$ m is the classical radius of proton, A is the mass number of the ion, a_h and a_v are the horizontal and vertical radii of the beam. This expression is valid for a beam with uniform transverse distribution. For bi-Gaussian distribution [1], the right side of Eq. (3.4) should be multiplied by $\sqrt{2}$ when the substitutions $a_{h,v} = \sqrt{6}\sigma_{h,v}$ are made, where $\sigma_{h,v}$ are the rms horizontal/vertical beam size.

At the vacuum pressure of 3×10^{-5} Torr, the beam current in the transfer line is $I \sim 56.1$ mA (see Fig. 2). Thus the $\tau_b = 35$ μs H^- beam corresponds to a linear density of $\lambda_b = I/(e\beta c) = 2.92 \times 10^{10}$ m^{-1}. The H^- beam has a round cross section of radius $a_h = a_v = 1.0$ cm. This gives the resonant frequency of $\omega_i/(2\pi) = 1.43/\sqrt{A}$ MHz as tabulated in Table 2. In the table, the beam currents in the transfer line at various gas pressures are obtained by linearizing the experimental current plot in Fig. 2 with $I = 61$ and 39 mA at 1×10^{-5} and 1×10^{-4} Torr, respectively.

To compare with the experimental data, we show in Figs. 5, 6, 7, and 8 the spectra of the beam oscillations for hydrogen, helium, nitrogen, and argon. Unlike Fig. 3, these plots are in linear scale so that the resonant peaks can be read off more easily.

The resonant frequencies computed in Table 2 are in the neighborhood of 1 MHz, in qualitative agreement with the experimental resonant frequencies depicted in Figs. 5 to 8. The observed resonant peaks in general have wide spreads. This may be because of the nonuniformity of the linear distribution of the H^- beam as well as the variation of its transverse radius.

On the other hand, there are also disagreements with theory. Definitely, we do not see the $A^{-1/2}$ dependency given by Eq. (3.4). However, in computing the resonant frequencies in Table 2, we have assumed only singly charged ions.

Table 2: Ion-beam resonant frequencies according to Ref. [1] for gases at various vacuum pressures or beam currents.

Gas	H	He	N	Ar	Kr
Mass number A	1	4	14	39	84
Resonant frequency (MHz)					
at 1×10^{-5} Torr (61.0 mA)	1.490	0.745	0.398	0.236	0.163
at 2×10^{-5} Torr (58.6 mA)	1.460	0.730	0.390	0.231	0.159
at 3×10^{-5} Torr (56.1 mA)	1.429	0.715	0.382	0.226	0.156
at 4×10^{-5} Torr (53.7 mA)	1.398	0.699	0.374	0.221	0.153
at 5×10^{-5} Torr (51.2 mA)	1.366	0.683	0.365	0.216	0.149
at 6×10^{-5} Torr (48.8 mA)	1.333	0.666	0.356	0.211	0.145
at 7×10^{-5} Torr (46.3 mA)	1.299	0.649	0.347	0.205	0.142
at 8×10^{-5} Torr (43.9 mA)	1.264	0.632	0.338	0.200	0.138
at 9×10^{-5} Torr (41.4 mA)	1.228	0.614	0.328	0.194	0.134
at 1×10^{-4} Torr (39.0 mA)	1.192	0.596	0.319	0.188	0.130

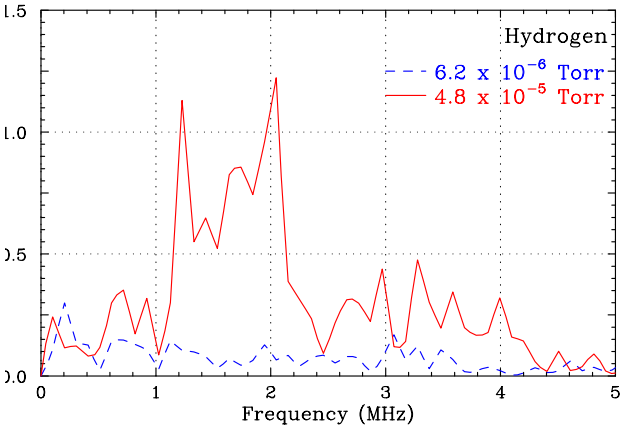

Figure 5: FFT of H^- beam horizontal displacement averaged over many beam pulses when hydrogen is introduced. Note that there is no coherent instability when the vacuum pressure is 6.2×10^{-6} Torr.

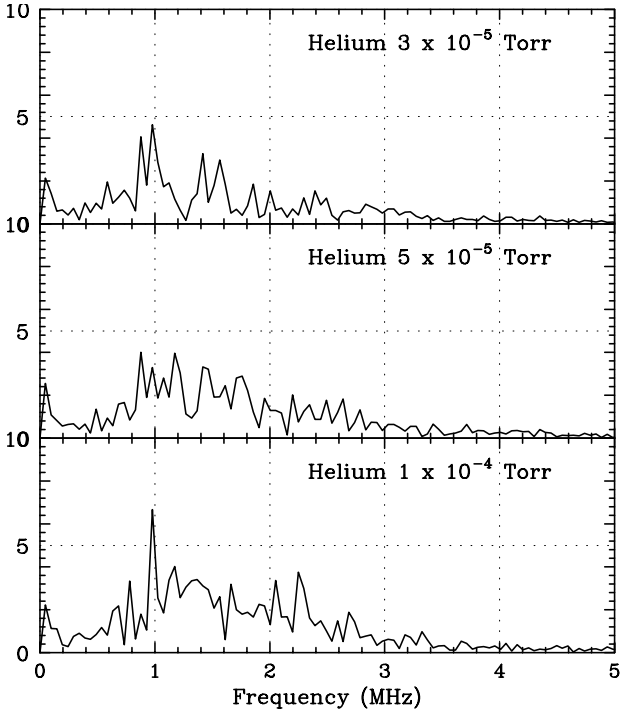

Figure 6: FFT of H^- beam horizontal displacement averaged over many beam pulses. Helium is the gas introduced. The frequency spread does not depend much on gas pressure.

Because the velocity of the incident H^- are much greater than those of the electrons in the outermost shells of the various gases, the ionization cross sections do not depend much on the ionization energy. There are, for example, 6 electrons in the outermost shell of an argon atom or krypton atom, it will be as easy for two or more electrons to be knocked off as for one. If there were doubly or triply charged ions produced, the resonant frequency would have been $\sqrt{2}$ and $\sqrt{3}$ times larger. It is very plausible that the deviation of the $A^{-1/2}$ dependency for argon and krypton is due to the production of multi-charged ions.

The expression, Eq. (3.4), is independent of the gas pressure. The slight decrease of the resonant frequency with rising pressure tabulated in Table 2 is just a reflection of the H^- current or linear density as a result of possible stripping by the gas particles. For the experiment data, we see in Figs. 5 and 7 that the resonant frequencies for helium and nitrogen do not depend much on pressure. For argon, Fig. 8 indicates that the frequency distributions are more or less the same for gas pressure from 3×10^{-6} to 5×10^{-6} Torr. However, we do clearly see the resonant peak become wider and move towards higher frequencies as the gas pressure increases to pass 5×10^{-5} Torr.

Unfortunately experimental data for krypton have not been digitized and we need to look into scope displays in Fig. 9. We see that for gas pressure below 4×10^{-5} Torr, there is a resonant peak near 0.5 MHz. As the gas pressure increases to 1×10^{-4} Torr, the resonant peak shifts towards higher frequencies, close to 1 MHz.

For hydrogen, Fig. 5 shows that there is no transverse instability at the normal operating pressure of 6.2×10^{-6} Torr. When the pressure is increased to 4.8×10^{-5} Torr, two resonant peaks appear at 1.2 and 2.1 MHz, with the former very close to the theoretical prediction. Results with higher gas

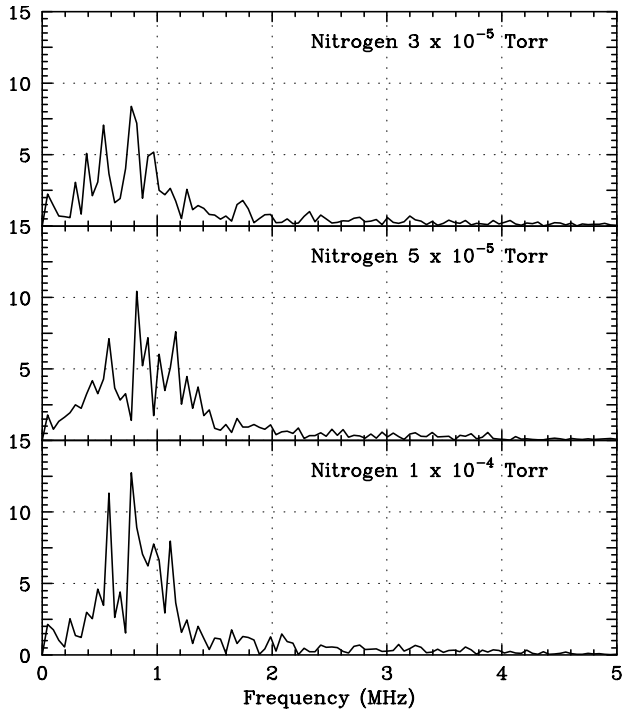

Figure 7: FFT of H^- beam horizontal displacement averaged over many beam pulses. Nitrogen is the gas introduced. The frequency spread does not depend much on gas pressure.

pressures were not available because it had not been able to maintain a stable gas pressure with hydrogen; the large ion pumps are efficient only for pumping gases of higher masses.

In summary, we find that the resonant frequency is not sensitive to pressure for light gases like helium and nitrogen. However, for the heavier gases such as argon and krypton, the resonant peaks are broadened and move towards higher frequencies when the pressure is larger than $\sim 5 \times 10^{-5}$ Torr. To conclude, we plot the spreads of the experimental resonant frequencies of the different gases for all the pressures studied in Fig. 10. On the same plot we also include the resonant frequencies computed in Table 2 from 1×10^{-5} Torr (top trace) to 1×10^{-4} Torr (bottom trace). From the figure, it is evident that the theoretical predictions, as a whole, underestimate the experimental results.

3.3 Growth Times

With some assumptions[1], the linear theory of Raubenheimer and Zimmermann leads to a simple solution. After entering the residual gas environment for time t, the horizontal oscillation amplitude $\tilde{x}_b$ of the beam at a distance τ (measured in time) behind the head is given by [1]

$$\tilde{x}_b(t,\tau) = x_0 I_0(\eta) \,, \tag{3.5}$$

where $x_0 = \tilde{x}_b(0,0)$ is the initial horizontal displacement of the head of the beam, I_0 is the modified Bessel function

[1] see Sec. 4.2 below

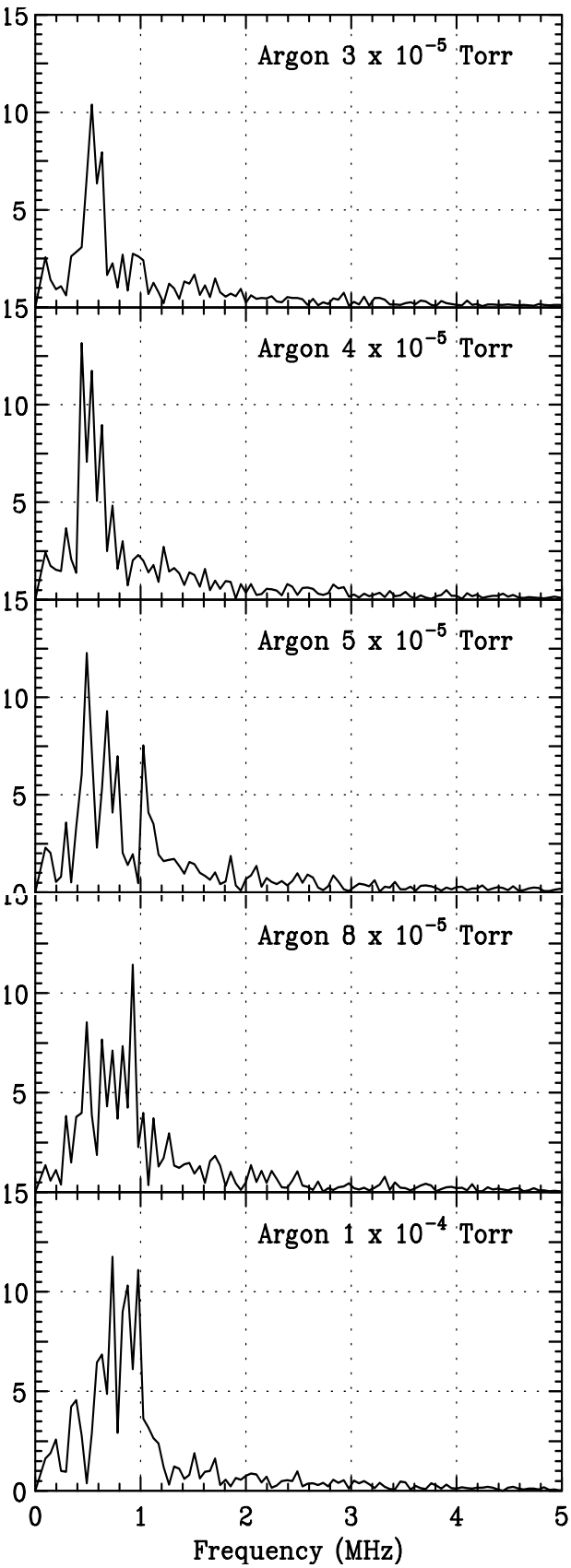

Figure 8: FFT of H^- beam horizontal displacement averaged over many beam pulses. Argon is the gas introduced. The resonant peak becomes broadened as the gas pressure increases and moves towards higher frequencies.

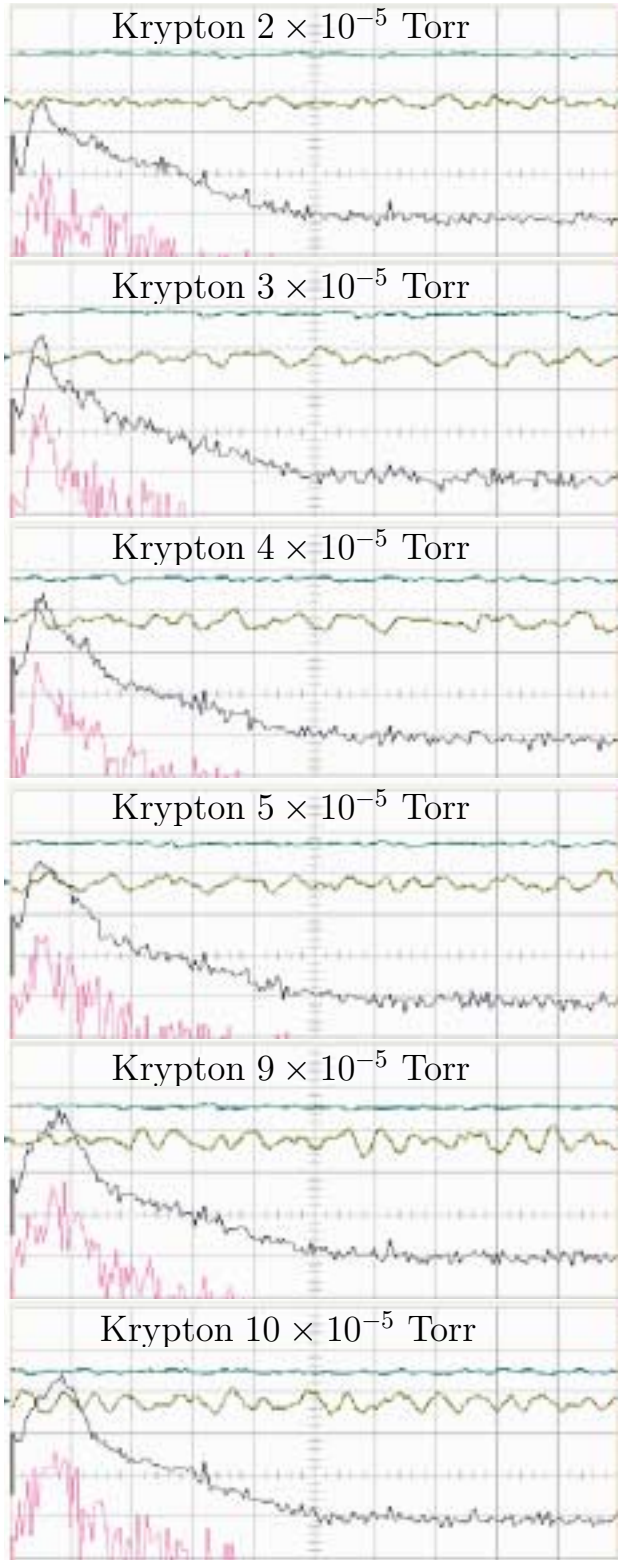

Figure 9: (color) Scope displays of the H^- beam when krypton is injected at various pressures. The second trace at 2 μs per division is the horizontal displacement of the H^- beam starting from the 14 th μs to the end of the beam pulse. Its FFT at 1 MHz per division is the third trace and has been averaged over 20 beam pulses. The resonant peak becomes broadened at higher pressures and tends to move towards higher frequencies.

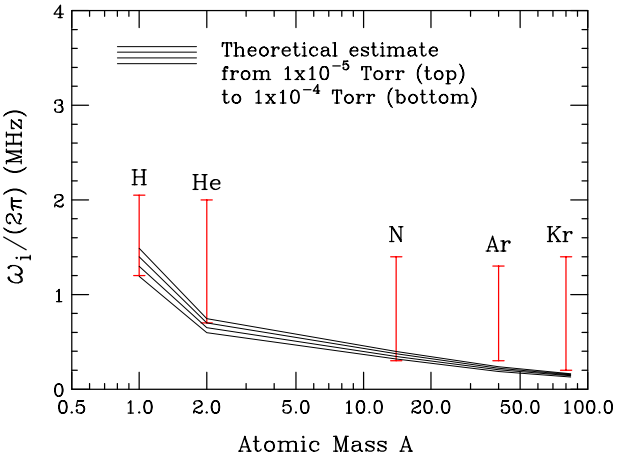

Figure 10: Spreads of measured resonant frequencies of different gases at all the pressures studied. The theoretical predictions from 1×10^{-5} Torr (top trace) to 1×10^{-4} Torr (bottom trace) are also shown.

of order zero, and

$$\eta = \frac{\tau}{\tau_b}\sqrt{\frac{t}{t_0}} \tag{3.6}$$

is a dimensionless function of t and τ. In the asymptotic regime where $\eta \gg 1$, we have

$$\tilde{x}_b(t,\tau) \approx x_0 \frac{e^\eta}{\sqrt{2\pi\eta}} \,. \tag{3.7}$$

Thus, t_0 plays the role of a growth time although the evolution is actually not exponential in t. This growth time is related to the ion bounce frequency by

$$t_0 = \frac{2\omega_\beta}{\omega_b^2 \omega_i \tau_b} \,. \tag{3.8}$$

In above, $\omega_\beta/(2\pi)$ is the betatron frequency of the particle beam along the transfer line and $\omega_b/(2\pi)$ is the bounce frequency of the beam particles about the ions near the tail of the beam pulse where ions, produced cumulatively from the head of the beam to its tail, have the largest linear density λ_i. In other words,

$$\omega_b^2 = \frac{8\lambda_i r_p c^2}{\gamma a_h (a_h + a_v)} \,, \tag{3.9}$$

where λ_i is computed according to

$$\lambda_i = \Sigma n_g N_b \,, \tag{3.10}$$

with N_b being the total number of particles in the beam and Σ the ionization cross section tabulated in Table 1. The gas particle density n_g, on the other hand, can be derived from the ideal gas law

$$n_g = \frac{pN_A}{RT} \,, \tag{3.11}$$

where $N_A = 6.022 \times 10^{23}$ is the Avogadro's number, p is the gas pressure in atm (1 atm = 760 Torr), $T = 300°$K is

the room temperature, and $R = 82.55 \times 10^{-6}$ atm-m^3-K^{-1} is the gas constant.

Comparing the beam particle bounce frequency ω_b in Eq. (3.9) with the ion bounce frequency ω_i in Eq. (3.4), there is first an extra γ in the denominator because the beam particles are moving longitudinally, and second the factor 8 in the numerator while it was only 4 for the ion bounce frequency. The latter is due to the fact that the ions, when produced, are assumed without any transverse velocity and start to oscillate about the particle beam. Since the largest transverse amplitude of oscillation is the particle beam radii, the radii of the "ion beam" will be relatively smaller than those of the particle beam. Simple derivation leads to the result that the rms radii of the ions are $a_{h,v}/2$. On the other hand, the rms radii of the uniformly distributed H^- beam are $a_{h,v}/\sqrt{2}$. Thus the radii of the "ion beam" are just a factor $\sqrt{2}$ smaller than the radii of the H^- beam. Although Eq. (3.9) is for a beam with uniform distribution, however, it gives exactly the same value for a bi-Gaussian distribution if we assume $a_{h,v} = \sqrt{6}\sigma_{h,v}$, with $\sigma_{h,v}$ being the rms radii of the beam.

Assuming periodicity, the phase advance of the $\ell \sim 10$ m transfer line from the first large ion pump to the 90° bend into the linac is 443° in the horizontal plane and 110° in the vertical plane. Thus, an estimate of the horizontal betatron frequency is $\omega_\beta/(2\pi) = (\beta c/\ell)(443/360) = 1.47$ MHz. The growth time t_0 is then computed at a chosen reference pressure of 1×10^{-5} Torr, and the results for different gases are listed in Table 3. First, at this pressure, the beam current in the transfer line is ~ 61 mA, giving a linear density of $\lambda_b = 3.18 \times 10^{10}$ m^{-1} and total number of beam particle $N_b = 1.33 \times 10^{13}$. Second, the residual gas density is $n_g = 3.22 \times 10^{17}$ m^{-3} and the ions produced have a linear density of $\lambda_b = 1.83 \times 10^{10}$ m^{-1}. The beam bounce angular frequencies ω_b are then computed and listed in Table 3. Finally the growth times t_0 are derived.

The transverse displacement of the H^- beam was measured by the BPM after Tank 2 in the linac. The excitation of transverse oscillation had been going on in the $\ell_t \sim 10$ m of the 750 keV transfer line from the chopper to the big ion pump near the entrance into the linac. Thus the time for which the beam can actually generate and interact with the ions is $t \sim \ell_t/(\beta c) = 0.835$ μs. We can define another *growth time along the beam* at the BPM as

$$\tau_0 = \tau_b \sqrt{\frac{t_0}{t}} \tag{3.12}$$

so that the asymptotic horizontal oscillation amplitude of the beam at the BPM, where t is fixed, becomes

$$\tilde{x}_b(\tau) \sim \exp\left(\frac{\tau}{\tau_0}\right) . \tag{3.13}$$

It is important to point out that τ_0 is independent of the length of the beam pulse τ_b or the location along the beam. This is because ω_b^2 in Eq. (3.9) is proportional to the ion density λ_i at the end of the beam and therefore proportional to τ_b. On the other hand, the growth time t_0 depends on the location along the beam, because it describes the growth of that location of the beam as time evolves. Actually, the end of the beam, $\tau = \tau_b$, has been chosen as a reference in the definition of t_0 in Eq. (3.8), which gives $t_0 \propto \tau_b^{-2}$.

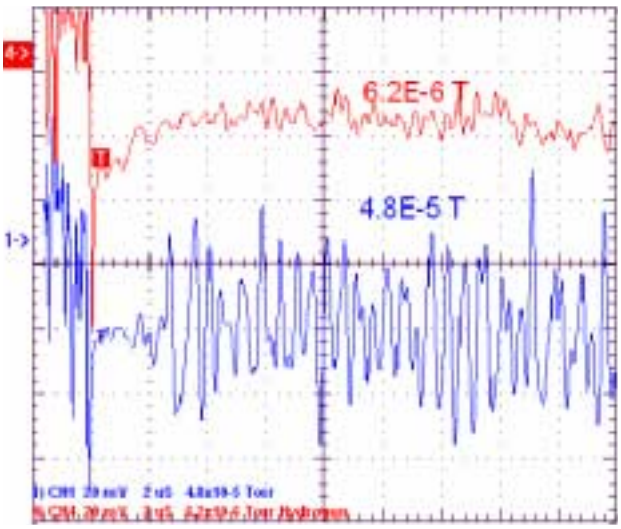

Figure 11: (color) Plot showing the H^- beam relatively stable inside a hydrogen environment at 6.2×10^{-6} Torr. However, at 4.8×10^{-5} Torr, the horizontal beam oscillation amplitude increases rapidly along the beam.

These growth times along the beam, τ_0, at the pressure of 1×10^{-5} Torr are listed in the last row of Table 3. For other pressure p, τ_0 scales as $p^{-1/2}$. The beam current should also be adjusted correspondingly. Figure 11 shows the beam transverse displacements in hydrogen for the first 18 μs. The beam appears to be stable at the pressure of 6.2×10^{-6} Torr. However, it grows to saturation in ~ 5 μs at 4.8×10^{-5} Torr. The theoretical prediction of the growth time along the beam is $\tau_0 = 0.46$ μs. Figure 12 shows the beam transverse displacements in helium. The theoretical predictions of the growth times along the beam are $\tau_0 = 0.99$, 0.82, and 0.71 μs at, respectively, 3, 5, and 10×10^{-5} Torr. The experimental growth times appear to be comparable. Figure 13 shows the beam transverse displacements in nitrogen. The theoretical predictions of the growth times along the beam are $\tau_0 = 0.71$, 0.44, 0.39, and 0.39 μs at, respectively, 1.5, 5, 8, and 10×10^{-5} Torr. The experimental growth times appear to be longer, especially at lower pressures. Figure 4 shows the beam transverse displacements in argon. The theoretical predictions of the growth times along the beam are $\tau_0 = 0.82$, 0.73, 0.68, 0.60, and 0.59 μs at, respectively, 3, 4, 5, 8, and 10×10^{-5} Torr. Again, the experimental growth times appear to be longer especially at lower pressures. For krypton, the theoretical predictions of the growth times along the beam are $\tau_0 = 0.89$, 0.79, 0.74, 0.65, and 0.64 μs at, respectively, 3, 4, 5, 8, and 10×10^{-5} Torr. However, there have not been any recorded beam displacement data for krypton at the early part of the beam. What Fig. 9 shows are only the

Table 3: Computation of growth time along the H^- beam at 1×10^{-5} Torr. The growth time at other pressure p scales with $p^{-1/2}$.

	H	He	N	Ar	Kr
ω_b (MHz)	10.1	8.00	20.2	17.3	19.1
Growth time at end of beam pulse t_0 (μs)	0.00056	0.00177	0.00052	0.00120	0.00142
Growth time along beam τ_0 (μs)	0.91	1.61	0.87	1.33	1.44

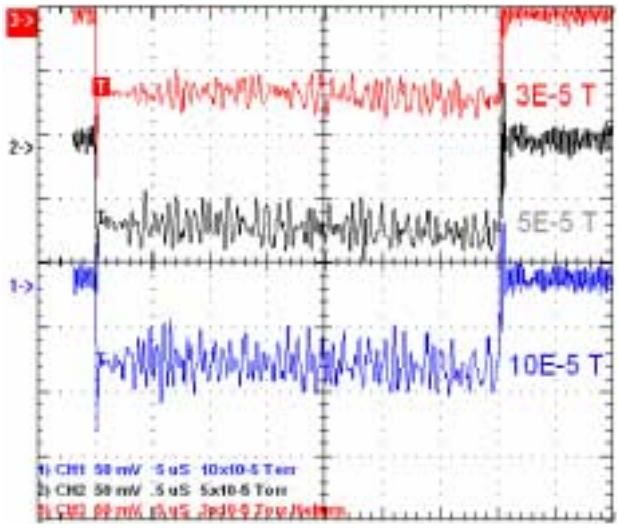

Figure 12: (color) Plot showing rapid growth of beam horizontal oscillation amplitude at various helium pressures.

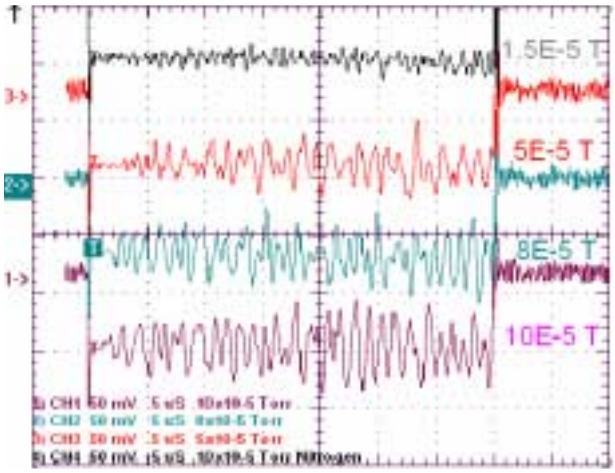

Figure 13: (color) Plot showing rapid growth of beam horizontal oscillation amplitude at various nitrogen pressures.

beam displacements starting from the 14th μs. As a result, no comparison of experiment with theory can be made for the growth time in krypton.

4 COMMENTS

4.1 *The Different Environments*

The beam-ion environment here is very different from that in an electron ring. Some relevant quantities are listed in Table 4. We see a huge difference:

1. The ion bounce frequency in an electron ring is very much larger because of much higher electron linear density and the much smaller transverse electron beam size.

2. There are very much more ions produced in the Fermilab linac than in an electron ring. The ion linear density in an electron ring is negligibly small compared with the beam linear density, while in the Fermilab linac the ion linear density is of the same order as the beam linear density. This is due to the much higher residual gas pressure and larger ionization cross section in the transfer line where the H^- are traveling with a small velocity. As a result, the beam bounce frequency in the ions becomes very much smaller in an electron ring.

3. There are 3 frequencies in the fast beam-ion instability theory, the ion bounce frequency $\omega_i/(2\pi)$, the beam bounce frequency $\omega_b/(2\pi)$, and the betatron frequency $\omega_\beta/(2\pi)$. For the two situations,

$$\begin{array}{ll} \text{Electron ring} & \omega_i \gg \omega_\beta \gg \omega_b \\ \text{Fermilab linac} & \omega_b \gtrsim \omega_\beta \gtrsim \omega_i \,. \end{array} \tag{4.14}$$

4.2 *Validity of the Linear Theory*

Because of the difference, close examination of the fast beam-ion instability is necessary in order to find out whether the linear theory applies to the transfer line of the Fermilab linac. In order to arrive at the simple solution of Eq. (3.5), an approximation has been made. The equation governing the beam oscillation amplitude $\tilde{x}_b(t,\tau)$ at some stage of the derivation is given by

$$\frac{\partial}{\partial t}\tilde{x}_b(t,\tau) + \\ + \frac{i\omega_b^2}{2\omega_\beta\tau_b}\int_0^\tau d\tau'\,\tau'\left[\frac{\partial}{\partial\tau'}\tilde{x}_b(t,\tau') + \frac{i\omega_i}{2}\tilde{x}_b(t,\tau')\right] = 0\,, \tag{4.15}$$

which is a modification of Alex Chao's Eq. (4.32) in Ref. [10]. The first term in the square brackets is neglected, leading to

$$\frac{\partial}{\partial t}\frac{\partial}{\partial\tau}\tilde{x}_b(t,\tau) - \frac{\omega_b^2\omega_i\tau}{4\omega_\beta\tau_b}\tilde{x}_b(t,\tau) = 0\,. \tag{4.16}$$

Table 4: Comparison of some beam and ion parameters in a typical electron ring and in the Fermilab linac, assuming that CO is the residual gas.

	Electron Ring	Fermilab Linac Experiment	
Number per bunch N_b	10^{11}	1.3×10^{13}	
Bunch length ℓ_b	0.010	419	m
Beam radius	0.001	0.010	m
Beam linear density λ_b	10^{13}	3.2×10^{10}	m^{-1}
Residual gas pressure	10^{-9}	1×10^{-5}	Torr
Gas-in-beam linear density λ_{gas}	1×10^{8}	1.0×10^{14}	m^{-1}
Ionization cross section for CO Σ	2	133	Mb
Maximum ion linear density λ_i	640	5.7×10^{10}	m^{-1}
CO^+ ion bounce frequency $\omega_i/(2\pi)$	64	0.40	MHz
Beam bounce frequency† $\omega_b/(2\pi)$	0.00092	2.82	MHz

†10 GeV electrons are assumed for electron ring.

Introducing the new dimensionless variable η of Eq. (3.6), the differential equation then simplifies to the Bessel equation

$$\eta \frac{d^2\tilde{x}_b}{d^2\eta} + \frac{d\tilde{x}_b}{d\eta} - \eta\tilde{x}_b = 0 \,, \tag{4.17}$$

and therefore the Bessel function solution of Eq. (3.5) is obtained.

Now let us examine whether the above approximation can be made in our situation. When we are talking about growth time, we are looking in the asymptotic behavior, like Eq. (3.7), or when $\eta \gg 1$, which is well satisfied when we are considering a position along the beam which is a few growth times behind the head. The neglect of the first term in the square brackets therefore requires the satisfaction of

$$\frac{\omega_i \tau_0}{2} \gg 1 \,. \tag{4.18}$$

In Fig. 14, we plot $\frac{1}{2}\omega_i\tau_0$ as a function of pressure for the different gases. It is clear that criterion in Eq. (4.18) is satisfied for hydrogen and helium when the pressure is low and becomes marginal when the pressure is higher than 5×10^{-5} Torr. For nitrogen, argon, and krypton, the criterion fails. This implies that the concept of a growth time τ_0 given by Eq. (3.12) may not be valid for these heavier gases. Therefore, we cannot say whether the results for nitrogen, argon, and krypton agree with the linear theory of fast beam-ion instability or not. A more sophisticated solution of Eq. (4.15) must be obtained without the deletion of the first term in the square brackets before further comparison with experiment can be made for these heavier gases.

Even for hydrogen and helium, the resonant frequency is around 1 MHz and less, and the passage time through the 10 m transfer line is 0.835 μs. This implies that the beam and the ion made less than one oscillation about each other. It is hard to visualize how a coherent instability can be established within such a short time. This is another reason why we are skeptical whether the expression for growth time could be applied to our experiment.

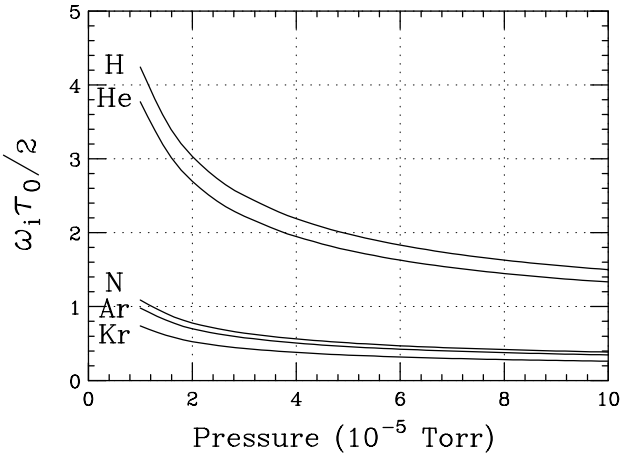

Figure 14: Plot of $\frac{1}{2}\omega_i\tau_0$ versus gas pressure for various gases. When $\frac{1}{2}\omega_i\tau_0 \gg 1$, the neglect of the first term inside the square brackets of Eq. (4.15) is justified leading to the exponential asymptotic solution of Eq. (3.7). Since the requirement is not satisfied for nitrogen, argon, and krypton, the concept of the growth time given by Eq. (3.12) may not be correct.

5 CONCLUSION

We reported a beam-ion instability experiment in the 750 keV transfer line of the Fermilab linac, and compared the results with the linear theory of fast beam-ion instability conjectured by Raubenheimer and Zimmermann. What we found are:

1. The coherent resonant frequencies observed are around 1 MHz, which agree qualitatively with, although relatively larger than the prediction of the

linear theory of the fast beam-ion instability.

2. We did not see a drop of the resonant frequency according to the inverse square root of the mass number A of the gas inserted. The rather slower drop may imply the generation of multiply charged ions by the H^- beam.

3. We observed that the resonant peak is relatively independent of gas pressure for light gases such as helium and nitrogen. However, the resonant peak is broadened and moves towards higher frequencies at higher gas pressure for the heavier gases such as argon and krypton. This dependence is not predicted by the linear theory of fast beam-ion instability. We suspect that as the gas pressure increases, more variety of beam-gas interactions become available producing other resonant peaks at slightly higher frequencies.

4. The growth of the oscillation amplitude along the beam appears to be initially exponential-like along the beam as predicted by theory, but rapidly saturates due possibly to nonlinearity. The growth times observed tend to be somewhat larger than what the theory predicts. This is completely possible, however, if damping mechanisms are involved, for example, decoherence due to a spread in the resonant frequency. It would be nice if these damping meachanics could be established experimentally and theoretically, so that the effective growth times could derived.

5. Experiments demonstrating fast beam-ion instability have been performed at various electron rings [9]. However, the experimental observations and result analysis are usually complicated by the presence of electron clouds formed from secondary emission and multi-pactoring. Because of the absence of electron clouds in the Fermilab linac transfer line, our experiment is very much cleaner.

6. One questionable parameter used in the analysis is the betatron frequency $\omega_\beta/(2\pi)$. First, the transfer line is not a ring and the lattice does not possess periodicity. The phase advance actually depends on the initial displacement and divergence of the particle. Whether a betatron frequency can be defined in this context is very questionable. Second, the average phase advance turns out to be only 443° in the horizontal plane, or the beam particles make just more than one oscillation in their passage through the transfer line. We are also skeptical that coherent oscillations can be established in about one betatron oscillation.

7. The linear theory of fast beam-ion instability may not be applicable to the transfer line H^- beam in the environment of heavier gases like nitrogen, argon, and krypton. Because the criterion $\frac{1}{2}\omega_i\tau_0 \gg 1$ is not satisfied, the approximation of ignoring a term in the derivation of the growth time will therefore not be justified. A more general solution of the differential equation governing the evolution of the beam oscillation amplitude is necessary for more precise comparison with experiment.

At this moment, it is not possible to conclude that the observed beam-ion instability observed in the 750 keV transfer line of the Fermilab linac is the fast beam-ion instability conjectured by Raubenheimer and Zimmermann. This is because what have been measured are only the coherent resonant frequencies and the growth times along the beam, and the agreement of these measurements with the linear theory is far from complete satisfactory. It has also been suggested that the large amount of ions generated by the H^- beam together with the stripped electrons create a plasma [11]. The H^- beam, which may be less intense than the plasma, produces a perturbation in the plasma, drives the electrons away and is neutralized by the positively charged ions nearby. Such interaction can also generate a coherent transverse oscillation between the H^- beam and the plasma. In any case, further experimental study is necessary to better understand this observed instability.

6 REFERENCES

[1] T.O. Raubenheimer and F. Zimmermann, Phys. Rev. **E52**, 5487 (1995).

[2] E. McCrory, G. Lee, and R. Webber, *Observation of Transverse Instabilities in FNAL 200 MeV Linac*, Proceedings of 1988 Int. Linac Conf. 3-7 October 1988, Williamsburg, VA.

[3] I.A. Soloshenko, *Space Charge Compensation and Collective Processes in the Intensive Beams of H^- Ions*, AIP Conf. Proceedings **380**, 1995, pp 345.

[4] M.D. Gabovich, V.P. Goretsky, D.G. Dzhabbarov, and A.P. Naĭda, Institute of Physics of Ukrainian Science Academy **N 9**, Kiev, 1979, pp 18.

[5] M. Popovic and T. Sullivan, *Observation of a H^- Beam Ion Instability*, Proceedings of XX Int. Linac Conf. 21-25 August 2000, Monterey, CA.

[6] H. Bethe, Ann. Physik **5**, 325 (1930).

[7] M. Inokuti, Rev. Mod. Phys. **43**, 297 (1971).

[8] F.F. Rieke and W. Prepejcjal, Phys. Rew. **A6**, 1507 (1972).

[9] J. Byrd, et al., Phys. Rev. Letter. **79**, 79 (1997); M. Kwon, et el., Phys. Rev. **E57**, 6016 (1998).

[10] A.W. Chao, *Lecture Notes on Topics in Accelerator Physics*, US Particle Accelerator School, 5-16 June 2000, SUNY Stony Brook, New York, available at http://www.slac.stanford.edu/∼achao/lecturenotes.html
Our equation comes from Eq. (4.32), where the two independent variables are replaced by $s = \beta ct$ and $z = \beta c\tau$, $\tilde{y}$ is replaced by $\tilde{x}$, K is replaced by ω_b^2, and a factor β is inserted into the denominator just before the integral sign and also one into the denominator just before the closing square bracket.

[11] V. Dudnikov, private communication; see also Refs. [3] and [4].